Crystal Chemistry of $LuPd_2O_4$ and Other Spinel-Related $NdCu_2O_4$−$LaPd_2O_4$-Type Compounds

Bai-Hao Chen* and Dave Walker

Lamont-Doherty Earth Observatory of Columbia University, Palisades, New York 10964

Bruce A. Scott

IBM Thomas J. Watson Research Center, Yorktown Heights, New York 10598

Received March 13, 1997. Revised Manuscript Received May 2, 1997[⊗]

Lutetium palladium oxide ($LuPd_2O_4$) has been prepared in a multianvil apparatus at 60 kbar pressure and 1000 °C. It crystallizes in the tetragonal $LaPd_2O_4$-type structure with space group $I4_1/a$, $a = 5.681(1)$ Å, $c = 9.881(2)$ Å, and $Z = 4$. The structure of this compound, like that of $NdCu_2O_4$ and other members of this new class, is closely related to that of spinel except for the difference in oxygen arrangements, leading to a difference in coordination of the A, B, and O ions. It can be derived from spinel by oxygen displacements. A new version of Kugimiya and Steinfink's AB_2O_4 correlation map in the region $0.04 < K_{ab} < 0.18$ and $0.8 < r_a/r_b < 1.7$, has been generated. It shows that the new AB_2O_4 class lies in the area between the spinel- and $CaFe_2O_4$-type regions.

Introduction

Compounds with the stoichiometry AB_2O_4 exhibit many structural types. The major structural types are spinel, olivine, phenacite, K_2MgF_4, K_2SO_4, $CaFe_2O_4$, and $BaAl_2O_4$. Recently, two new AB_2O_4 structural types, monoclinic $NdCu_2O_4$ with space group $I2/b$ (No. 15, unique axis c) and tetragonal $LaPd_2O_4$ with space group $I4_1/a$ (No. 88), have been discovered.[1−4] The compounds $LnCu_2O_4$ (Ln = Y, La, Nd, Sm, Eu, Gd, Er, and Lu) adopt the former, while the compounds RPd_2O_4 (R = Y, La, Pr, Nd, and Gd) and AAu_2O_4 (A = Ca, Sr, and Ba) crystallize in the latter. In addition, nonstoichiometric $NdCu_2O_4$-type cuprates $YCu_{1.8}O_y$ and $TmCu_{1.8}O_y$ have also been reported.[5] These new AB_2O_4 phases can only be prepared under high pressure, except for $LnCu_2O_4$ phases containing Ln with radii larger than that of Tm, which can also be obtained using low-temperature flux methods.[1] Although the crystal symmetries between $NdCu_2O_4$ and $LaPd_2O_4$ are different, their structures are essentially same. Both are related to spinel as described by Chen et al.[2] Recently, part of our research has been involving the search of new superconducting materials using high-pressure synthesis. The new AB_2O_4-class phases are of great interest to us not only because their structure is related to that of spinel but also because of B-site mixed valency (excluding B = Au) making these systems similar to mixed valence Ti^{3+}/Ti^{4+} in the superconducting spinel $LiTi_2O_4$.[6] In addition, from the geochemical point of view, the system is also of interest because some high pressure forms of the AB_2O_4 oxides are believed to be important constituents of Earth's mantle.[7] To explore the phase stability of the new AB_2O_4 classes and to improve our understanding of the structural relationship between them and spinel, we have carried out an investigation of the high-pressure synthesis and structure of $LuPd_2O_4$, using an octahedral multianvil apparatus and X-ray powder diffraction.

Synthesis and Structure of $LuPd_2O_4$

The $LuPd_2O_4$ phase was prepared from mixtures of Lu_2O_3 (Johnson Matthey, 99.99%), PdO (Cerac, 99.95%), and $KClO_3$ (Aldrich, 98%) as an oxygen source in molar ratio 3:12:1. Lu_2O_3 was prefired at 950 °C immediately before use. The mixture was ground, loaded in an Al_2O_3 capsule, and placed into a multianvil apparatus. The apparatus uses two stages, eight anvil cubes within six cubic anvil drivers, contained within a cylindrical stress guide. Uniaxial forces of up to 450 tons from a hydraulic press drive the compression of the sample within an octahedral solid ceramic pressure medium through the sliding system of the ring, wedges, and anvils. A full description of the multianvil apparatus and the high-pressure experimental procedures has been published previously.[8] The final product was obtained at 60 kbar and 1000 °C for 3 h.

The sample was characterized with a Siemens D-500 X-ray powder diffractometer using Cu Kα radiation. The X-ray powder data were obtained in the range $20° < 2\theta < 80°$ using a step width of 0.02°and a counting period of 20 s. The X-ray pattern is similar to $LaPd_2O_4$, suggesting that it has the $LaPd_2O_4$ structural type. The structure of $LuPd_2O_4$ was refined by Rietveld profile analysis of X-ray powder diffraction data using the FULLPROF program with a pseudo-Voigt peak-shape

[⊗] Abstract published in *Advance ACS Abstracts,* June 15, 1997.

(1) Keller, S. W.; Carlson, V. A.; Sandford, D.; Stenzel, F.; Stacy, A. M.; Kwei, G. H.; Alario-Franco, M. *J. Am. Chem. Soc.* **1994**, *116*, 8070.

(2) Chen, B.-H.; Walker, D.; Suard, E.; Scott, B. *Chem. Mater.* **1995**, *7*, 355.

(3) (a) Krämer, G.; Jansen, M. *J. Solid State Chem.* **1995**, *114*, 206. (b) Krämer, G.; Hägele, E.; Wagner, N.; Jansen, M. *Z. Anorg. Allg. Chem.* **1996**, *622*, 1027.

(4) (a) Krämer, G.; Jansen, M. *J. Solid State Chem.* **1995**, *118*, 247. (b) Park, J.-H.; Parise, J. B. *Chem. Mater.* **1995**, *7*, 1055.

(5) Tatsuki, T.; Adachi, S.; Itoh, M.; Tamura, T.; Wu, X.-J.; Jin, C.-Q.; Yamauchi, H.; Koshizuka, N.; Tanaka, S. *Jpn. J. Appl. Phys.* **1995**, *34*, L615.

(6) Johnston, D. C.; Prakash, H.; Zachariasen, W. H.; Viswanathan, R. *Mater. Res. Bull.* **1973**, *8*, 777.

(7) Reid, A. F.; Ringwood, A. E. *J. Solid State Chem.* **1970**, *1*, 557.

(8) (a)Walker, D. *Am. Mineral.* **1991**, *76*, 1092. (b) Chen, B.-H.; Walker, D.; Suard, E.; Scott, B.; Mercey, B.; Hervieu, M; Raveau, B. *Inorg. Chem.* **1995**, *34*, 2077.

S0897-4756(97)00150-6 CCC: $14.00

Table 1. Crystallographic Data for $LuPd_2O_4$ with Estimated Standard Deviations in Parentheses[a]

formula weight	451.77
crystal system	tetragonal
space group	$I4_1/a$ (No. 88)
a (Å)	5.681(1)
c (Å)	9.881(2)
V (Å^3)	318.9(1)
Z	4
D_c (g cm^{-3})	9.410
no. of reflections	52
R_P (%)	5.07
R_{wp} (%)	7.07
R_B (%)	1.84
R_E (%)	1.20

Positional and Isotropic Thermal Parameters

atom	site	x	y	z	B (Å^2)
Lu	4a	0	0.25	0.125	1.5(2)
Pd	8d	0	0	0.5	2.1(3)
O	16f	0.149(2)	0.072(2)	0.313(1)	1.0

Selected Bond Distances (Å) and Bond Angles (degree)

Lu−O	2.32(1) × 4	Lu−O	2.28(1) × 4		
Pd−O	2.07(1) × 2	Pd−O	2.02(1) × 2	Pd−Pd	2.840(1) × 2
O−Pd−O	81.3(3)	O−Pd−O	98.7(3)		
Lu−O−Lu	110.0(3)	Lu−O−Pd	131.6(4)	Lu−O−Pd	101.5(3)
Pd−O−Pd	102.2(3)	Lu−O−Pd	105.0(3)	Lu−O−Pd	103.4(4)

[a] $R_p = \sum|Y(i)_o - C*Y(i)_c|/\sum|Y(i)_o|$, $R_{wp} = \{\sum w(i)[Y(i)_o - C*Y(i)_c]^2/\sum w(i)*Y(i)_o^2\}^{1/2}$, $R_B = \sum|I(k)_o - I(k)_c|/\sum I(k)_o$, $R_E = \{(N - P + S)/[w(i)*Y(i)_o^2]\}^{1/2}$, where C is a scaling factor, N is the number of points in the pattern, P is the number of refined parameters, S is the number of strict constraint functions, $Y(i)$ are profile intensities after background subtraction, $I(k)$ are Bragg intensities, and $w(i)$ are weights.

Table 2. Lattice Parameters of the $NdCu_2O_4$ and $LaPd_2O_4$-Type Compounds

compound	a (Å)	b (Å)	c (Å)	γ (deg)	V(Å^3)	refs
			$NdCu_2O_4$ Type			
$LaCu_2O_4$	5.919(1)	5.846(1)	9.764(2)	92.24(1)	337.6	1
$NdCu_2O_4$	5.826(1)	5.753(1)	9.703(1)	92.34(1)	324.6	1
$NdCu_2O_4$	5.822(2)	5.748(2)	9.695(3)	92.34(2)	324.2	2
$SmCu_2O_4$	5.784(1)	5.707(1)	9.667(1)	92.42(1)	318.8	1
$EuCu_2O_4$	5.762(1)	5.684(1)	9.646(1)	92.40(1)	315.6	1
$GdCu_2O_4$	5.742(2)	5.663(2)	9.628(3)	92.40(2)	312.7	2
YCu_2O_4	5.695(2)	5.611(2)	9.569(3)	92.56(2)	305.5	2
$ErCu_2O_4$	5.668(2)	5.590(2)	9.548(3)	92.48(2)	302.2	2
$LuCu_2O_4$	5.624(2)	5.545(2)	9.507(3)	92.51(2)	296.2	2
			$LaPd_2O_4$ Type			
$LaPd_2O_4$	5.9140(5)		10.289(1)		359.9	3
$PrPd_2O_4$	5.8382(2)		10.1687(5)		346.6	3
$NdPd_2O_4$	5.8419(3)		10.1949(6)		347.7	3
$NdPd_2O_4$	5.830(3)		10.181(5)		346.0	*a*
$GdPd_2O_4$	5.7799(3)		10.0677(8)		336.3	3
YPd_2O_4	5.7359(3)		9.9829(8)		328.4	3
YPd_2O_4	5.727(3)		9.969(5)		327.0	*a*
$LuPd_2O_4$	5.684(2)		9.881(3)		318.8	*a*
$BaAu_2O_4$	6.4297(4)		10.251(2)		423.8	4
$SrAu_2O_4$	6.1830(1)		10.1704(2)		388.3	4
$CaAu_2O_4$	5.99114(1)		10.04983(3)		360.7	4

[a] This work (the samples were prepared at 60 kbar).

function.[9] The refinement parameters include atomic position, lattice parameters, a zero-point error, isotropic thermal parameters except that for oxygen, overall scale factor, background, peak-shape parameter, and half-width parameters. The input of the lattice parameters for the refinement was obtained by a least-squares method.[10] The structure of $LaPd_2O_4$ was used as the starting model. Impurities phases Pd, PdO, Lu_2PdO_4, Lu_2O_3, and KCl in the sample were also included in the refinement.

$LuPd_2O_4$ adopts the $LaPd_2O_4$ structural type and its crystallographic data are summarized in Table 1. The $LnPd_2O_4$ (Ln = Y and rare earth) series, including the new $LuPd_2O_4$ member, exhibits the following structural features: (a) the ratio of the lattice parameters c/a is a constant ∼1.743; (b) the Pd−O−Pd bond angles decrease with the size of Ln due to the decrease of the Pd−Pd distances, resulting in increasing metallic behavior;[3] (c) reducing the size of Ln also increases the electrostatic repulsion between oxygen ions, increasing the distortion (i.e., the difference between two Pd−O bond distances) of the PdO_4 square plane; (d) the average Ln−O distances are shorter than the sum of the Shannon's ionic radii due to the preparation under high pressure;[11] (e) the average Pd−O distances vary from 2.00 to 2.05 Å; (f) cell volumes depend on the synthesis condition. The cell volumes of the samples prepared at 60 kbar are smaller than those prepared at 20 kbar (see Table 2). Table 1 also shows that the average M−O−M (M = Pd or Lu) bond angle in the distorted Lu_2Pd_2O tetrahedra is 109.0°, compared to 109.5° for a regular tetrahedron.

Structural Relationship between the New AB_2O_4 Class and Spinel

The structure of the new AB_2O_4 class is presented in Figure 1a. Corner-sharing square planar BO_4 groups are linked perpendicularly to each other, leading to a parallel array of pseudotetragonal tunnels along the c-axis. A ions reside in these tunnels, forming distorted edge-sharing AO_8 triangulated dodecahedra. Figure 1b shows the structure is comprised of parallel stacks of BO_4 square planes running along the a and b axes. Oxygen links to two A and two B ions, forming distorted A_2B_2O tetrahedra (B−O−B angles, which are 90° for spinel, are close to 109.5°). In contrast, the structure of spinel presented in Figure 2a consists of edge-shared BO_6 octahedra and isolated AO_4 tetrahedra. Oxygen links to one A and three B ions, forming AB_3O polyhedra.

The structure of the new AB_2O_4-class is very similar to that of spinel. The unit-cell dimension of the former is related to that of the latter by $(\sqrt{2}/2)a_s \times (\sqrt{2}/2)a_s \times a_s$, where a_s is the lattice parameter of the cubic spinel. The lattice parameters of the new AB_2O_4-class phases are listed in Table 2. The cations in both structures have the Cu_2Mg Laves-type structure, in which the A ions occupy the Mg site, while the B ions occupy the Cu site.[12] However, their oxygen arrangements are different, leading to coordination of the A, B, and O ions as described previously. The change in coordination between these two structures can be derived by two operations. First, the BO_4 square planes parallel to the c-axis are tilted $\sim\pm\pi/8$ with respect to those of spinel (see Figures 1a and b). Second, the BO_4 planes perpendicular to the a and b-axes are rotated by $\sim\pm\pi/8$ with respect to those of spinel about the 4-fold axis of the BO_4 planes (see Figure 1b). The adjacent planes are rotated toward each other, forming distorted O_8 square antiprisms. Such oxygen displacements not only meet the coordination requirement for the new AB_2O_4 class but also reduce the electrostatic repulsion between oxygens.

The structural relationship between spinel and the new AB_2O_4 class is illustrated in Figure 2. As oxygen

(9) Rodriguez-Carvajal, J. Fullprof: A program for Rietveld refinement and profile matching analysis; Abstracts of the Satellite Meeting on Powder diffraction of the XV Congress of the International Union of Crystallography, Toulouse, France, 1990; p 127.

(10) Chen, B.-H.; Jacobson, R. A. *Powder Diffraction* **1990**, *5*, 144.

(11) Shannon, R. D. *Acta Crystallogr.* **1976**, *A32*, 751.

(12) Ohba, T.; Kitano, Y.; Komura, Y. *Acta Crystallogr.* **1984**, *C40*, 1.

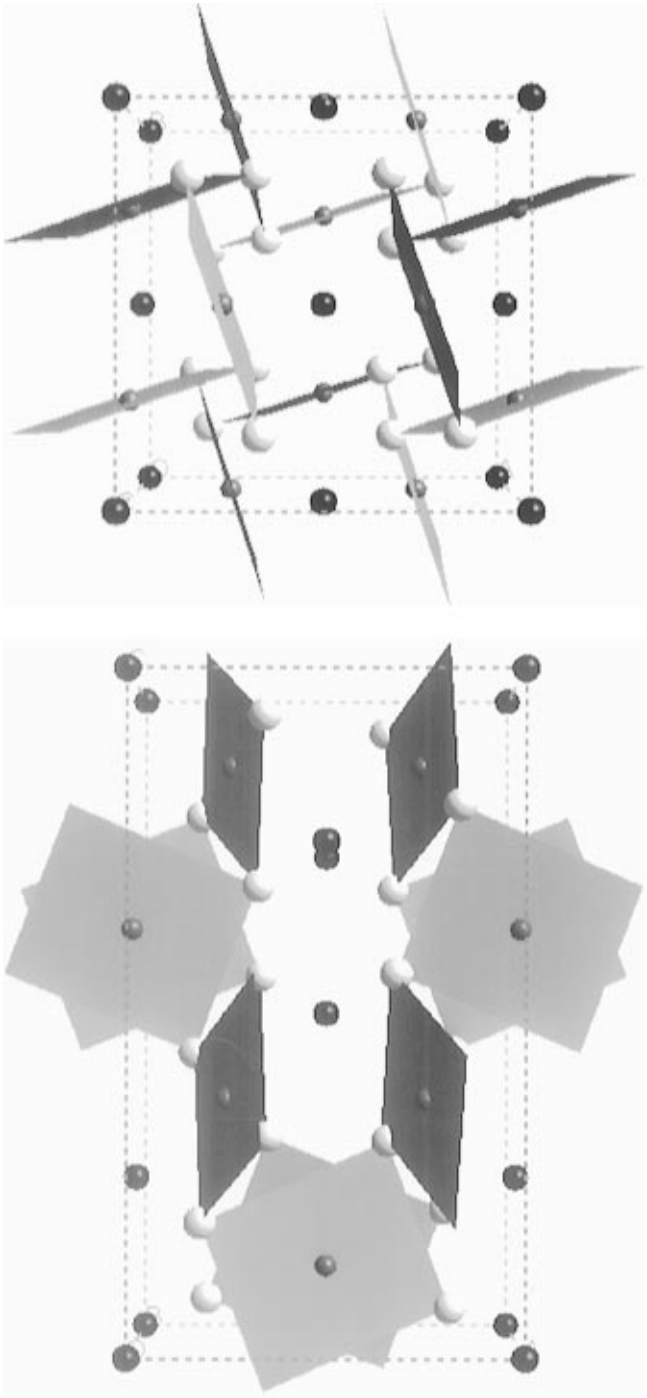

Figure 1. Structure of the new AB_2O_4-class, $LaPd_2O_4$–$NdCu_2O_4$-type. Medium (black), small (gray), and large (white) balls represent A, B, and O ions, respectively. (a, top) Projection on [001] (unique *c*-axis for monoclinic $NdCu_2O_4$), BO_4 square planes parallel to the *c*-axis are tilted $\sim\pm\pi/8$ with respect to those of spinel. (b, bottom) Projection on [100], BO_4 square planes perpendicular to the *a*-and *b*-axes are rotated by $\sim\pm\pi/8$ with respect to those of spinel about the 4-fold axis of the BO_4 planes.

ion O_a ($z = \sim 1/8$) in spinel (see Figure 2a) moves away from the B_3 ion toward one of the second-nearest A ions ($z = 0$), a distorted A_2B_2O tetrahedron forms (see Figure 2b). As a result, AO_4 tetrahedra in spinel transform to distorted edge-shared dodecahedra AO_8 in the $NdCu_2O_4$-class phases, while BO_6 octahedra transform to corner-shared BO_4 square-planes. The spinel structure transforms into the new AB_2O_4-class structure through this distortion.

New Version of Kugimiya–Steinfink AB_2O_4 Correlation Map

Kugimiya and Steinfink (K–S) have grouped the known structures for compounds with AB_2O_4 stoichiometry by plotting r_a/r_b versus the bond stretching force constant K_{ab} defined as:

$$K_{ab} = X_a X_b / r_e^2$$

where $r_e^2 = (r_a + r_o)^2 + (r_b + r_o)^2 + 1.155(r_a + r_o)(r_b + r_o)$ and r_a, r_b, and r_o are the radii of the A, B, and O ions, and X_a and X_b are the electronegativities of the A and B ions, respectively.[13] This K–S AB_2O_4 map provides a useful index to predict the structural types of unknown phases and led to the solution of the $NdCu_2O_4$-type structure.[2]

Using Shannon's six-coordinated ionic radii for the A, B, and O ions and Allred–Rochow's electronegative values,[11,14] the r_a/r_b, and K_{ab} values were computed for the spinel, $NdCu_2O_4$-, $LaPd_2O_4$-, and $CaFe_2O_4$-type phases in the region $0.04 < K_{ab} < 0.18$ and $0.8 < r_a/r_b < 1.7$. The B-cation radii (B = Cu and Pd) were taken by averaging those of B^{2+} and B^{3+}. It should be pointed out that the radii employed in this work are different from those used in the original K–S map.[13] In addition, the spinels which fall in the investigated region and $CaFe_2O_4$ phases from ref 15 were selected for mapping. On the basis of these r_a/r_b and K_{ab} values, a new K–S map was generated and is presented in Figure 3. The AB_2O_4 correlation diagram shows that the new AB_2O_4 types lie in the area between the spinel and $CaFe_2O_4$ regions and that the $NdCu_2O_4$- and $LaPd_2O_4$-type structures are distinguished by the force constant K_{ab}.

The $BaAu_2O_4$ and $CaIn_2O_4$ phases fall in unexpected fields in the new map. Although use of Pauling-type electronegativities can solve these problems,[16] they give poorer segregation between the new AB_2O_4 and spinel phases. Another popular AB_2O_4 correlation diagram besides the K–S map, plotting cationic radii A versus B, was produced by Muller and Roy.[15] To compare the Muller–Roy diagram with the K–S diagram, a new version of the former was generated. The results are far less encouraging for a correlation than the K–S mapping.

Summary

The $LaPd_2O_4$-type compound $LuPd_2O_4$ has been prepared under high pressure. Attempts to synthesize $ScPd_2O_4$ failed as did $ScCu_2O_4$,[2] suggesting that Sc ion is too small to occupy the A site in the $NdCu_2O_4$–$LaPd_2O_4$-type structure. The structure of the new AB_2O_4 class can be derived from that of spinel by oxygen displacements. The new Kugimiya–Steinfink AB_2O_4 correlation map shows that the radius ratio is a dominant factor in determining the structural type, while the electronegativity influences the symmetry. The distribution of crystallization types may be more complex than the model of the K–S map. Unsurprisingly, there are some violations on the map. However, it provides useful information for predicting the structure type of the AB_2O_4 phases falling into the spinel,

(13) Kugimiya, K.; Steinfink, H. *Inorg. Chem.* **1968**, *7*, 1762.
(14) Allred, A. L.; Rochow, E. G. *J. Inorg. Nucl. Chem.* **1958**, *5*, 264.
(15) Muller, O.; Roy, R. *The Major Ternary Structural Families*; Springer-Verlag: Berlin, 1974.
(16) Allred, A. L. *J. Inorg. Nucl. Chem.* **1961**, *17*, 215.

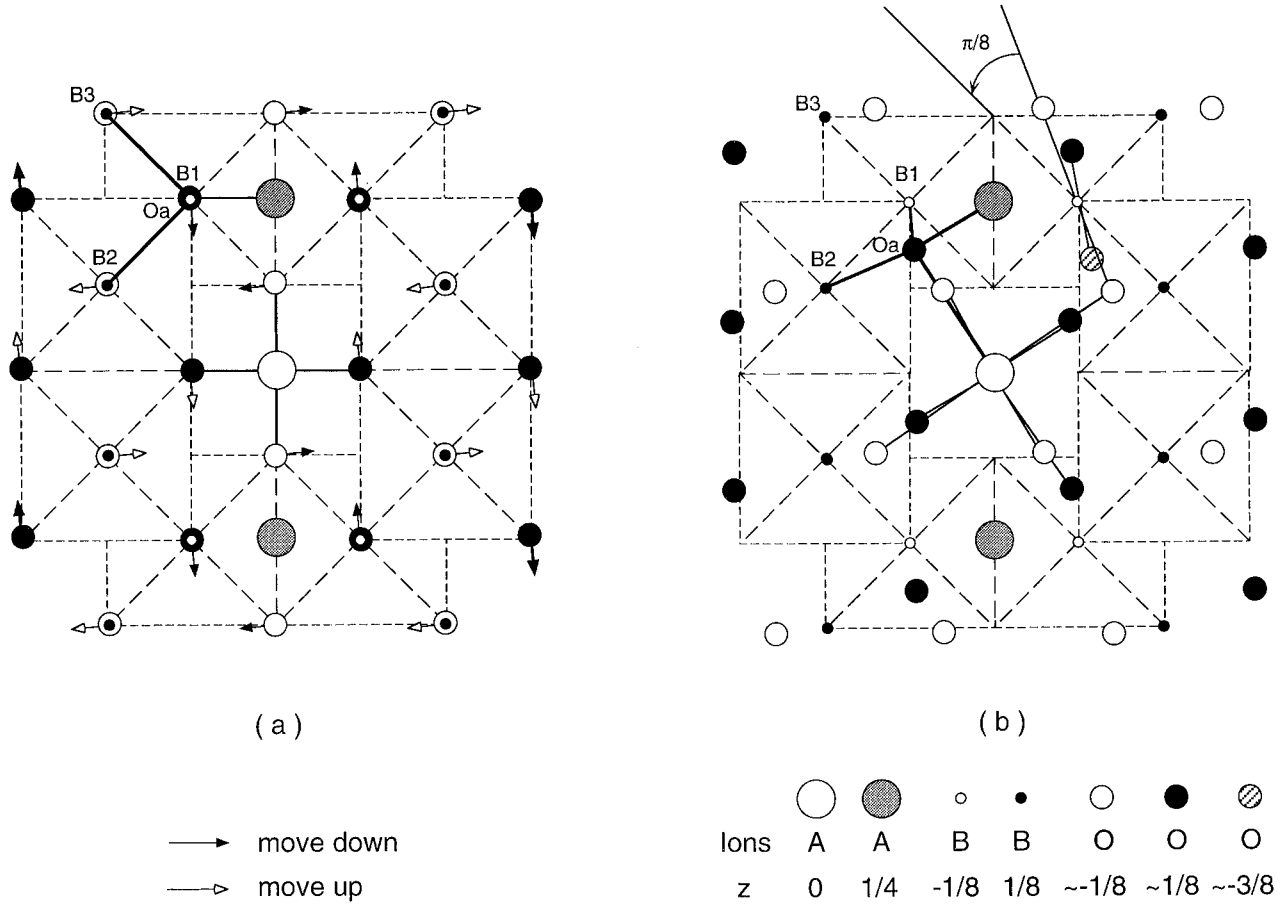

Figure 2. Structural comparison of spinel (a) and the new AB_2O_4 class, $LaPd_2O_4$−$NdCu_2O_4$-type, projected on [001] (unique *c*-axis for monoclinic $NdCu_2O_4$) (b). (a) Tetrahedra AO_4 (A at the center links to four oxygen ions), octahedra BO_6 (dash line), and AB_3O group (O_a links to A, B_1 ($z = -1/8$) below O_a, B_2, and B_3) in spinel. Arrows show the directions of the oxygen displacement from spinel to the new AB_2O_4 class. (b) Distorted dodecahedra AO_8, square planes BO_4, and A_2B_2O group (O_a links two A and two B) in the new AB_2O_4 class. BO_4 square planes are tilted $\sim\pi/8$ with respect to those of spinel.

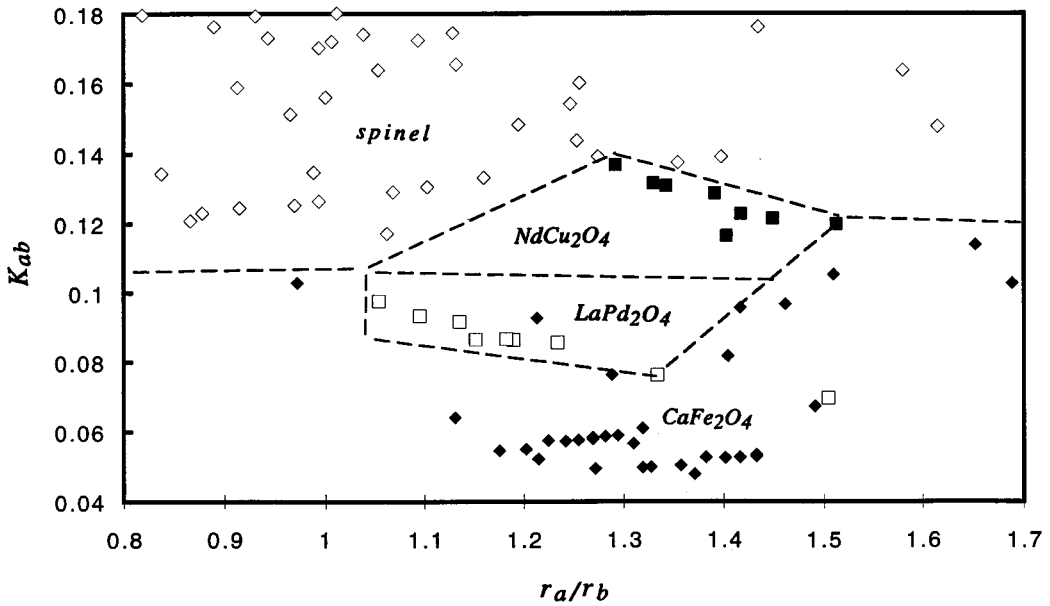

Figure 3. Kugimiya−Steinfink AB_2O_4 map for the spinel-, $LaPd_2O_4$-, $NdCu_2O_4$-, and $CaFe_2O_4$-type compounds. Open diamonds, black diamonds, open squares, and black squares represent spinel-, $CaFe_2O_4$-, $LaPd_2O_4$-, and $NdCu_2O_4$-type phases.

$NdCu_2O_4$, $LaPd_2O_4$, and $CaFe_2O_4$ regions of the K−S map, and for designing new materials with a desired structural type.

Acknowledgment. The authors wish to thank Mr. G. Paparoni for drawing Figure 2 and Ms. J. Hanley for technical assistance. This work is Contribution 5665 from the Lamont-Doherty Earth Observatory of Columbia University and was supported by the National Science Foundation and the Department of Energy. Work at the IBM Watson Research Center was supported by the Electric Power Research Institute.

CM970150H